Depths of Equivalent Dipole Polarizability Resolution for Some Transmitter Receiver Configurations

J Torquil Smith, H Frank Morrison, Alex Becker
Earth Sciences Division
Lawrence Berkeley National Laboratory
Berkeley, California 94720

ABSTRACT

Equivalent dipole polarizability matrices and equivalent dipole location are a convenient way to summarize magnetic induction data arising from currents induced in isolated conductive objects. The uncertainties in polarizability estimates and in equivalent dipole location provide a quantitative measure of the performance of different configurations of transmitters and receivers. Uncertainties in equivalent dipole polarizability matrices and equivalent dipole position are estimated using a linearized inversion. For a number of systems of rectangular loop transmitters and dipole receivers sited on a horizontal grid, equivalent dipole depth is determined to 10% approximately 20% deeper, than the polarizability matrix elements can be determined to the same precision. Systems that have a lower product of rms polarizability uncertainty and square root of their number of transmitter-receiver pairs are considered more effective for their number of transmitter-receiver pairs. Among the systems studied, a system with three orthogonal transmitter loops and a three component receiver is the most effective, for objects shallower than 0.6 times the instrument siting grid spacing, yielding an rms polarizability uncertainty 0.04 times that of a single transmitter single receiver system. At intermediate depths, a system with two vertical component receivers on the diagonal of a horizontal transmitter loop is most effective for its number of transmitter-receiver pairs, yielding an rms polarizability uncertainty 0.07 times that of a single receiver system. At depths greater than 2.5 times the siting grid spacing a 3 orthogonal loop transmitter with a single vertical component receiver is about the most effective for its number of transmitter-receiver pairs, yielding an rms polarizability uncertainty 0.08 times that of a single transmitter system.

INTRODUCTION

Equivalent dipoles have long been used for approximating potential fields in geophysics as well other fields. Recently, they have been used to model secondary magnetic fields arising from currents induced in isolated conductive, and possibly magnetic bodies, for discrimination between unexploded ordnance (UXO) and other materials, for example, by Khadr *et al*. (1998), Bell *et al*. (2001), Pasion and Oldenburg (2001), or Baum (1999). In these recent examples, the induced dipoles are modelled as linearly proportional to the inducing magnetic fields at the body centers, related to each other by equivalent dipole polarizability matrices.

Equivalent dipole polarizability matrices and dipole locations are a convenient way to summerize active source induced current magnetic field measurements in an interpretable form. The matrices' principal moments give information on the rotational symmetry of a conductive object, their principal directions yield the object's orientation, and the dipole location $\mathbf{r}_o$ estimates the object's center position. Estimation of the polarizability matrix and equivalent dipole position is a non-linear inverse problem. Here uncertainty estimates from a linearized inversion are used to compute the depths to which the polarizability matrices and dipole locations can be estimated for steel spheres of varying radius, for several transmitter-receiver configurations.

EQUIVALENT DIPOLE POLARIZABILITY MATRICES

Equivalent dipole polarizability matrices **M** model observed secondary magnetic fields $\mathbf{B}^{(s)}(\mathbf{r},t)$, in terms of the magnetic fields of unit dipoles in the $\hat{\mathbf{x}}$, $\hat{\mathbf{y}}$, and $\hat{\mathbf{z}}$ directions, $\mathbf{B}_x^{(d)}(\mathbf{r})$, $\mathbf{B}_y^{(d)}(\mathbf{r})$, $\mathbf{B}_z^{(d)}(\mathbf{r})$, centered at some location $\mathbf{r}_o$, and the primary (inducing) magnetic field strength $\mathbf{B}^{(o)} \cdot g(t)$, at $\mathbf{r}_o$, for a given time variation $g(t)$ of primary magnetic field:

$$\mathbf{B}^{(s)}(\mathbf{r},t) = \left[\mathbf{B}_x^{(d)}(\mathbf{r}), \mathbf{B}_y^{(d)}(\mathbf{r}), \mathbf{B}_z^{(d)}(\mathbf{r}) \right] \; \mathbf{M}(t) \; \mathbf{B}^{(o)} \quad . \tag{1}$$

The polarizability matrix is symmetric and is independent of transmitter and receiver geometry and object location. Its principal values are properties of the object, independent its orientation.

When the equivalent dipole position $\mathbf{r}_o$ is known, secondary magnetic field values depend linearly on the unknown polarizability matrix **M**, and may be estimated by minimizing the misfit to secondary magnetic field observations (data) for primary fields with at least three linearly independent orientations $\mathbf{B}^{(o)}$ at the equivalent dipole location. When the equivalent dipole position is unknown, the same procedure may be used at a series of canditate equivalent dipole positions, calculating the minimum data misfit attainable for each canditate position, and some search strategy used to find the position with lowest attainable data misfit.

Once the lowest attainable data misfit has been found, uncertainties in the resultant polarizability matrix and equivalent dipole location may be estimated from the partial derivatives of the observed data with respect to the model parameters. Uncertainty estimates are based on a perturbation analysis and are strictly accurate in the limit of small observation errors.

METHOD

An iterative linearized inversion was used to estimate equivalent dipole polarizabilities from synthetic three component magnetic field data for a vertical magnetic dipole source at 13 sites placed symmetrically on a rectangular grid above steel spheres of varying radius, modelled with a conductivity of $\sigma = 10^7 \; \Omega^{-1} m^{-1}$ and relative permeability $\mu_r = 180$, at 610 μs after transmitter current turnoff. In each case, variation between estimated principal moments is less than 3%, and less than 1% for spheres smaller than 25 cm radius, in agreement with the spheres' isotropy. All subsequent computations are based on these estimated moments, with the three estimated principal moments replaced by their average, which is indicated on the y-axis of Figure (1).

Computing principal moments and directions requires knowing all elements of **M**. A simple measure of how well a data set resolves **M** is the total squared uncertainty ε ;

$$\varepsilon^2 \equiv \sum_{i=1}^{3} \sum_{j=1}^{3} var(m_{ij}) \quad , \tag{2}$$

where $var(m_{ij})$ is the estimated squared uncertainty of the ij'th element of **M** obtained from the diagonal of the covariance matrix of the elements of **M**.

In general, polarizability variance estimates $var(m_{ij})$ depend on the specific values (realization) of noise in a data set, through partial derivatives of the data with respect to model parameters. In inversion of field data, the partial derivatives are evaluated at the minimum of misfit to the data. With a different set of errors in the data, slightly different partial derivatives would be evaluated at the position of the minimum misfit to the new data. In evaluating system performance, one can eliminate the

dependence of variance estimates on any particular noise realization, by evaluating partial derivatives at the true parameter values. All quantities plotted in the current paper are based variance estimates of this type.

For a given transmitter-receiver configuration, the polarizability variance and uncertainties are independent of the scale of the polarizability matrix, so, for a given instrumental configuration one need only calculate polarizability moment uncertainties once for any particular ratios of principal polarizabilities, orientation of principal directions, and object position. For spheres, one need only calculate moment uncertainties once for a given location of sphere relative to the instrument configuration. Similarly, uncertainty estimates for equivalent dipole location scale inversely with the object's polarizability matrix.

For each of a number of transmitter-receiver configurations, the total uncertainty ε was computed as a function of sphere depth, for spheres directly below the center of a 9x9 grid of system placements with 0.4 m spacing in x and y. One meter square transmitter loops were used with a moment of 180 Amp-m^2, and a receiver noise level of 1.97 nT/s in vertical field measurements, simulating an observed noise level, and 5.91 nT/s in horizontal field components (when present) simulating the larger noise levels observed in horizontal components.

RESULTS

Uncertainties in the diagonal elements of the polarizability matrix are plotted as a function of depth below transmitter and receiver in Figure (1), together with the total uncertainty ε, for isotropic equivalent dipole polarizabilities (spheres) below the grid of system placements for a horizontal loop transmitter/concentric vertical magnetic dipole receiver system. Being based on a linearized inversion for $\mathbf{M}$ and $\mathbf{r}_o$, these uncertainty estimates scale linearly with receiver noise level. The total moment uncertainty ε reaches a minimum near a depth of 0.14 meters. For shallower spheres, the uncertainties in m_{xx}, m_{yy}, and off diagonals m_{xy}, m_{yz}, m_{xz} (not shown) increase greatly approaching the plane of the transmitter and receiver, as all the transmitter placements illuminate the sphere with nearly vertical primary fields, yielding less information on these moments, and correspondingly large variances in them. Comparing the plotted values with the 610 μs polarizabilities of steel spheres of various radii, which are indicated on the left, the total uncertainty at shallow depths is considerably smaller than all indicated sphere polarizabilities. Since spheres have three equal principal moments, one can easily convert the total uncertainty ε to relative uncertainty, by dividing by $\sqrt{3}$ times the indicated polarizabilities. For a 6 cm radius steel sphere at 610 μs the relative uncertainty reaches 0.1 (10%) at 1.47 m depth. The corresponding relative uncertainties in horizontal and vertical polarizabilities are 0.061, 0.061, and 0.147 respectively.

Relative uncertainties in vertical location and horizontal location are plotted as a function of depth below transmitter and receiver in Figure (2), for an isotropic polarizability corresponding to a 6 cm radius steel sphere at 610 μs, for the same transmitter-receiver system as in Figure (1), on the same grid of system placements. These uncertainties can be scaled to correspond to other radius spheres by dividing by the ratio of polarizabilities of the spheres. Both horizontal and vertical uncertainties have been normalized by the depth to the equivalent dipoles. Because of symmetry of the transmitter and receiver, and of the sampling grid, uncertainties in x and y are identical. The relative uncertainty in depth reaches a 0.1 (10%) level by 1.83 m depth.

Because of the great range in the size of uncertainties in both equivalent dipole polarizability and location, it can be difficult to see differences in uncertainties when comparing plots for different

transmitter-receiver systems. For comparison purposes, it is convenient to plot the depth to some level of relative uncertainty for isotropic polarizabilities corresponding to spheres of varying radius. The depths to 5, 10, and 20% uncertainty in polarizability $d^{(p)}_{5\%}$, $d^{(p)}_{10\%}$, and $d^{(p)}_{20\%}$, were found for isotropic polarizabilities corresponding to spheres with radii between 1 cm and 1 m, and are plotted in Figure (3), as a function of sphere radius. The depths to 5, 10, and 20% uncertainty in estimated sphere depth, $d^{(z)}_{5\%}$, $d^{(z)}_{10\%}$, and $d^{(z)}_{20\%}$, are plotted in Figure (4). Object position can be estimated more precisely than the full polarizability matrix, as object position may be determined when an object is illuminated by only a single orientation of primary field, whereas estimating the full polarizability matrix requires illuminating the object with primary fields $\mathbf{B}_o$ in at least three directions, each with a significant component in the direction orthogonal to the other two. Object depth can be resolved within 10% to greater depths than polarizability in all cases plotted. Most cases presented here are for spherical objects. For comparison $d^{(p)}_{10\%}$ and $d^{(z)}_{10\%}$ are plotted in Figure (5) for the same transmitter-receiver pair, for the case of objects with the same vertical dipole polarizabilities $d\,m_{zz}/dt$ at 610 μs as spheres of the same radius, and all other polarizabilities null, corresponding to thin horizontal non-magnetic discs. The general trends are the same as for the sphere. Polarizability can be resolved to 10% slightly deeper than for the sphere for all but the smallest moment plotted. Object depth can be resolved approximately 1.2 times deeper than for the sphere.

Effects of adding a second coaxial vertical receiver 0.4 m above the first are shown in Figure (6), where $d^{(p)}_{10\%}$ and where $d^{(z)}_{10\%}$ are plotted for the two receiver system (dotted) together with their values for the previously plotted single receiver system (solid). In addition to resolving polarizabilities and location to greater depth as shown here, the added receiver makes locating the object position an easier problem as it eliminates a secondary minimum in data misfit near the true object position (not shown).

Figure (7) plots $d^{(p)}_{10\%}$ and $d^{(z)}_{10\%}$ (both dotted) for a similar system with the two vertical component receivers in the plane of the transmitter loop, offset ±0.2 m in x and y along a diagonal from the loop center. This system shows greatest improvement in sensitivity over the single receiver system for objects close to the transmitter-receiver plane, greatly increasing the depths to which the smallest spheres can be resolved.

Results for a horizontal loop transmitter three component concentric receiver are shown in Figure (8) (dotted lines). For comparison, a system with a 1 m^2 horizontal loop and two orthogonal 1 m^2 vertical loop transmitters with lower edges at the level of the horizontal loop is shown in Figure (9) (dotted lines). The results for the 3 transmitter 1 receiver system are substantially better than for the 1 transmitter 3 receiver system, in part, because of the greater noise level in horizontal component receivers.

As a final example, adding 2 orthogonal horizontal component receivers to the 3 transmitter system to make a 3 transmitter 3 receiver system yields results shown in Figure (10). The added horizontal components substantially increase the depth of resolution of the 1 cm radius sphere, but little affect results for 3 cm radius and larger spheres.

When averaging n measurements of a single kind of data, uncertainty in the average decreases as $1/\sqrt{n}$, so one expects a decrease on the order of $(n_r n_t)^{-½}$ for a system with n_t transmitters and n_r receivers. To compensate for this, total moment uncertainty ε multipled by $(n_r n_t)^{½}$ is plotted in Figure (11) as a function of sphere depth. The differences between curves mean that adding transmitters or receivers can reduce the uncertainty in the polarizabilty matrix by substantially more than is to be expected solely from an increase in the number of data.

For spheres above 0.26 m depth, the system with most receiver-transmitter pairs close to the object (three orthogonal loop transmitters and a 3 component receiver), gives the lowest $\varepsilon \cdot (n_r n_t)^{1/2}$ product, achieving a moment uncertainty 22.8 times smaller than the single transmitter single receiver system for spheres at 0.1 m depth. Between 0.26 to 1.0 m, as sphere depths become commensurate with the sampling grid spacing (0.4 m), the system with two vertical component receivers along the diagonal of the transmitter loop (of Figure 7) gives the lowest $\varepsilon \cdot (n_r n_t)^{1/2}$ product. At 0.5 m depth near where their ratio of uncertainties is greatest, the two vertical component receiver uncertainty is a factor of 13.6 times smaller than the single transmitter single receiver system uncertainty. Below 1.0 m the 3 orthogonal transmitter loop vertical component receiver (of Figure 9) gives the lowest $\varepsilon \cdot (n_r n_t)^{1/2}$ product; at 2.0 m depth, this system reduces the uncertainty by a factor of 11.8 compared to the single transmitter single receiver system. With the last system, adding additional vertical component receivers within the horizontal transmitter loop can result in $\varepsilon \cdot (n_r n_t)^{1/2}$ curves that are lower than the single receiver system curve at some depths, but in all cases that we have examined, the improvements in $\varepsilon \cdot (n_r n_t)^{1/2}$ between 1 m and 5 m are fairly marginal.

CONCLUSION

The polarizability matrix **M** and equivalent dipole polarizability location are best determined for objects at depths on the order of the system placement grid spacing or less. Determining all elements of the polarizabilty matrix **M**, to be able to compute its principal components, is a more demanding task than determining equivalent dipole polarizability location. Adding additional sources or receivers can improve the resolving power of a single transmitter single receiver system, by factors substantially better than the simple reduction by $(n_r n_t)^{-1/2}$ due to the increased number of data. For objects shallower than the sampling grid spacing, adding additional receivers and transmitter polarizations both can substantially improve the precision of polarizability matrix and dipole location estimates. For objects a few times deeper than the sampling grid spacing, a 3 orthogonal-transmitter loop, single vertical component receiver system is about the most effective for its number of receiver-transmitter pairs.

ACKNOWLEDGEMENT

This work was supported by the US Department of the Army under Contract No. W74RDV93447299

REFERENCES

C. E. Baum, ‘‘Low frequency near-field magnetic scattering from highly conducting, but not perfectly conducting bodies,’’ in C. E. Baum, Ed., *Detection and Identification of Visually Obscured Targets*, Philadelphia: Taylor et Francis, ch. 6, pp. 163-217, 1999.

T. H. Bell, B. J. Barrow, and J. T. Miller, ‘‘Subsurface discrimination using electromagnetic induction sensors,’’ *IEEE Trans. Geosci. Remote Sensing*, vol. 39, no. 6, pp.1286-1293. June 2001.

N. Khadr, B. J. Barrow, T. H. Bell, and H. H. Nelson, ‘‘Target shape classification using electromagnetic induction sensor data,’’ in *Proceeding of UXO Forum* 1998.

L. R. Pasion and D. W. Oldenburg, ‘‘Locating and determining dimensionality of UXOs using time domain elecromagnetic fields,’’ *Journal of Environmental and Engineering Geophysics*, vol. 6, no. 2, pp. 91-102, June 2001.

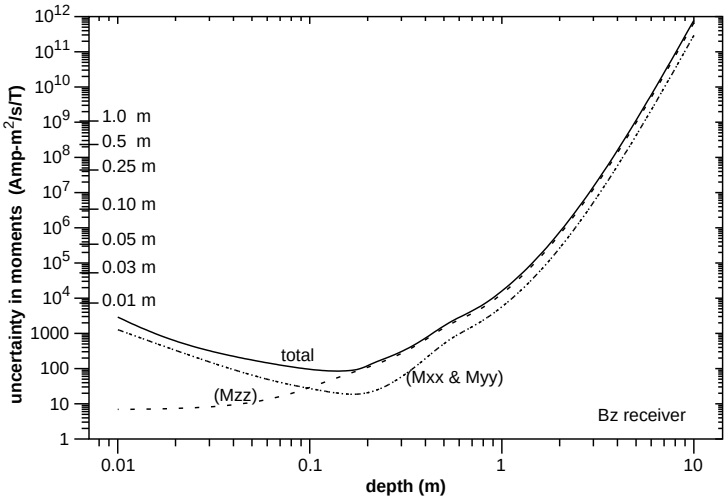

Figure (1). Total polarizability uncertainty ε (solid), as a function of sphere center depth below siting grid center, for a 1 m^2 square loop transmitter with a concentric vertical dipole receiver sited on a 9x9 grid with 0.4 m spacings. Uncertainty in vertical moment dm_{zz}/dt (dashed), and in horizontal moments dm_{xx}/dt and dm_{yy}/dt (dotted). Polarizabilities of steel spheres of various radii are indicted on left axis.

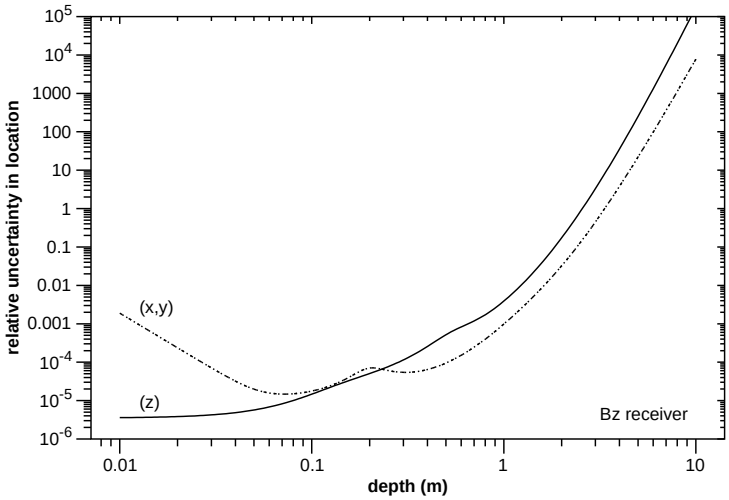

Figure (2). Relative uncertainty in equivalent dipole position, for a 0.641 Amp-m^2/s/μT isotropic polarizability as a function of depth below center of siting grid, for same system and grid as in Figure (1). Uncertainty in *z* (solid), uncertainty in *x* and *y* (dashed).

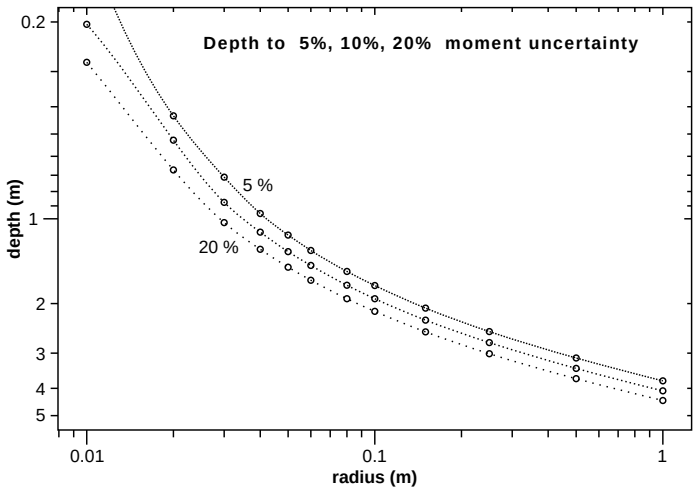

Figure (3). Depths to 5%, 10%, and 20% uncertainty in polarizability as a function of sphere radius for steel spheres, for same system and grid as in Figure (1).

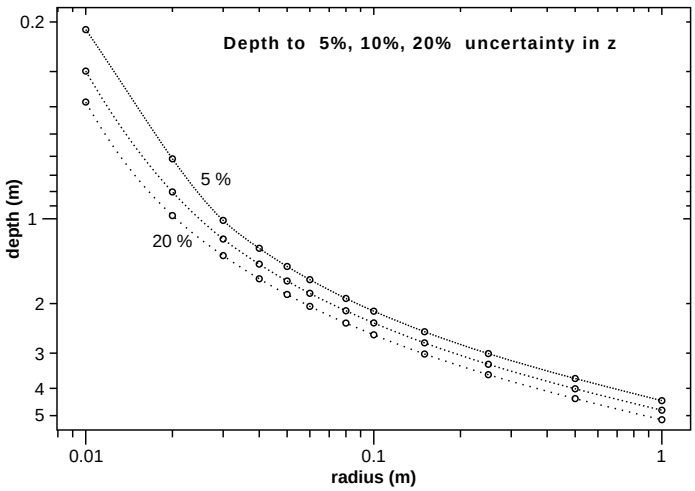

Figure (4). Depths to 5%, 10%, and 20% uncertainty in sphere center depth, as a function of sphere radius for steel spheres, for same system and grid as in Figure (1).

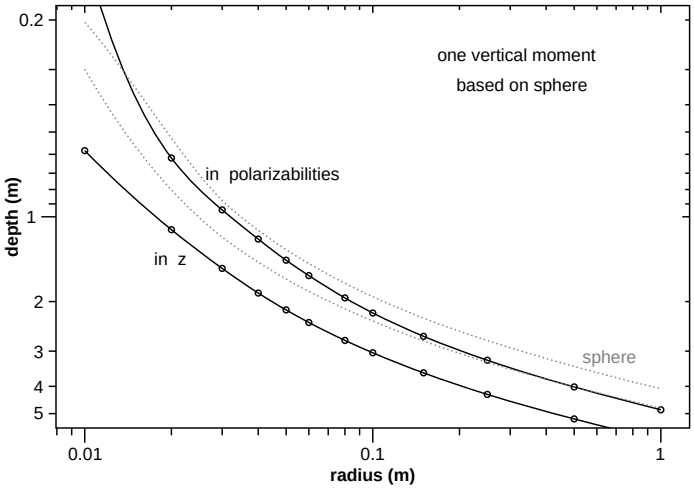

Figure (5). Depths to 10% polarizability uncertainty and to 10% uncertainty in center depth, for thin horizontal non-magnetic disk with same vertical polarizability dm_{zz}/dt at 610 μs, plotted as a function of the corresponding sphere's radius, for same system and grid as in Figure (1).

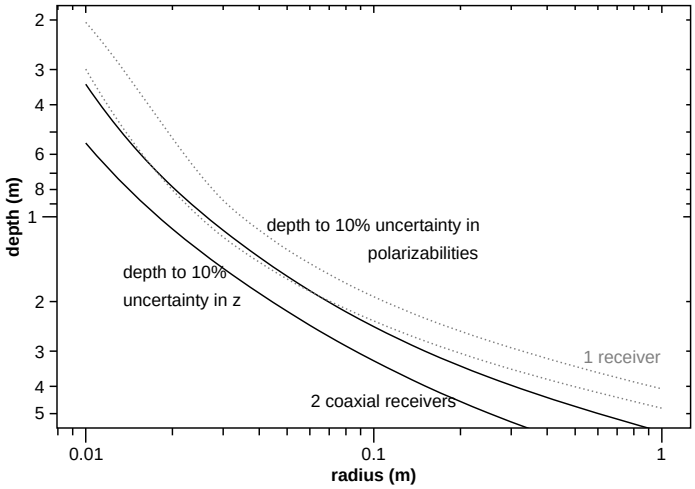

Figure (6). Depths to 10% polarizability uncertainty and to 10% uncertainty in center depth, as a function of radius for steel spheres below a 1 m^2 square transmitter loop with two coaxial vertical component receivers 0.4 m apart vertically, on same grid as in Figure (1).

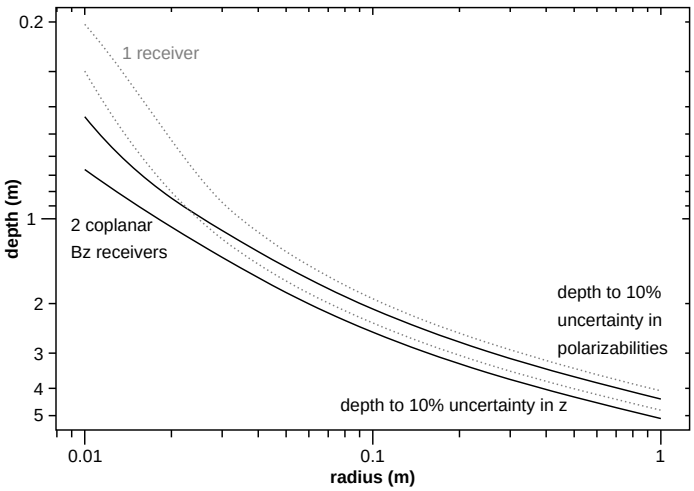

Figure (7). Depths to 10% polarizability uncertainty and to 10% uncertainty in center depth, as a function of sphere radius, for a 1 m^2 loop transmitter system with two vertical component receivers 0.566 m apart on diagonal in plane of transmitter loop, on same grid as in Figure (1).

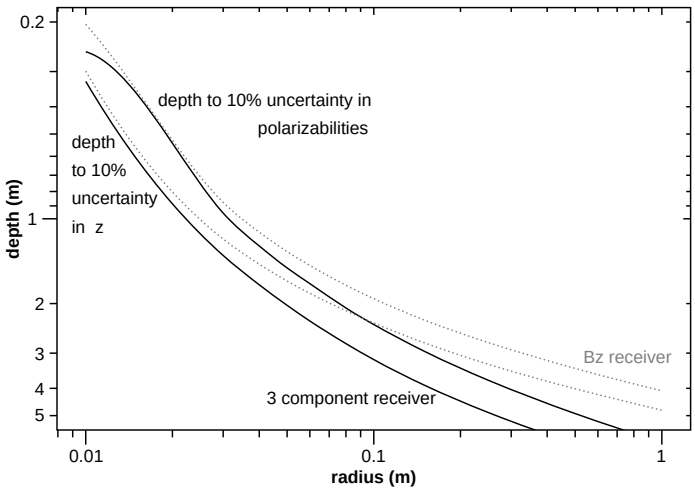

Figure (8). Depths to 10% polarizability uncertainty and to 10% uncertainty in center depth, as a function of sphere radius, for a 1 m^2 loop transmitter system with 3 component concentric receiver, on same grid as in Figure (1).

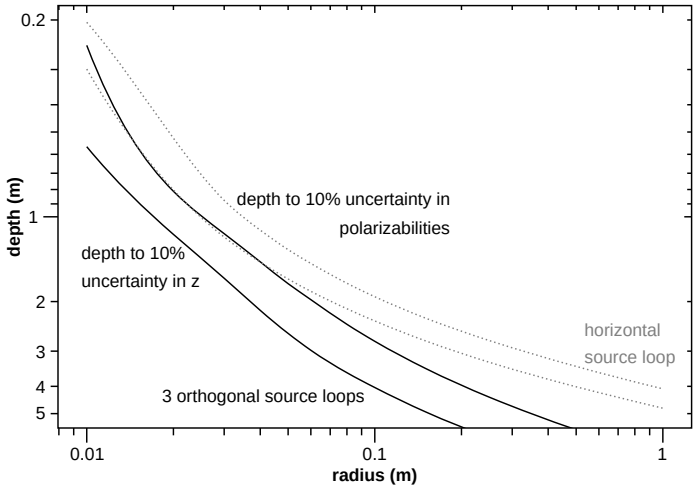

Figure (9). Depths to 10% polarizability uncertainty and to 10% uncertainty in center depth, as a function of sphere radius, for a 1 m^2 loop transmitter system with 3 component concentric receiver, on same grid as in Figure (1).

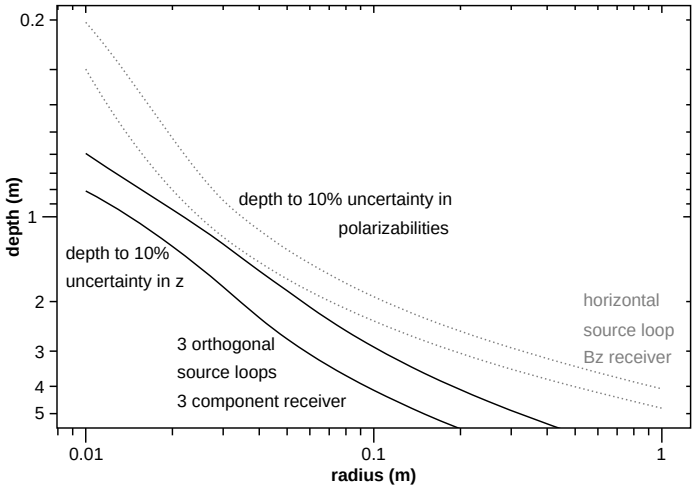

Figure (10). Depths to 10% polarizability uncertainty and to 10% uncertainty in center depth, as a function of sphere radius, for three orthogonal 1 m^2 transmitter loop system with vertical component receiver at horizontal loop center, on same grid as in Figure (1)

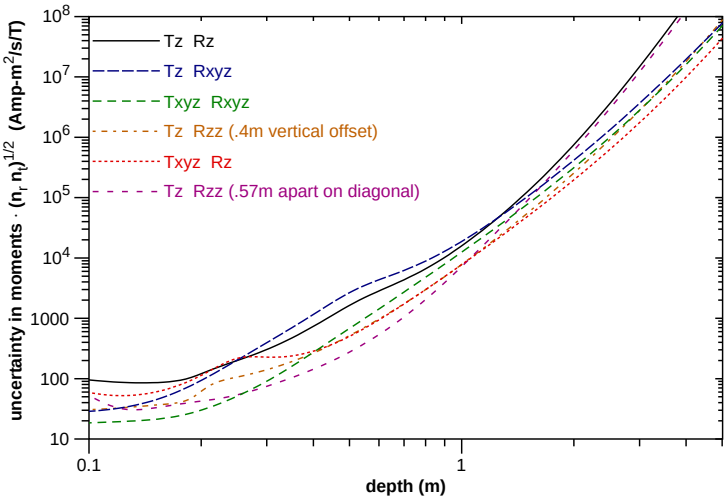

Figure (11). Total polarizability uncertainty ε divided by expected improvement $(n_r n_t)^{-1/2}$due increase in number of data, as a function of sphere center depth below center of system siting grid. (Solid) system of Figures (1)-(5). (Long dashes) system of Figure (8). (Medium dashes) system of Figure (10). (Dashed-dotted) system of Figure (6). (Dotted) system of Figure (9). (Short dashes) system of Figure (7).